Evaluation of stress field parameters for an interface crack in a bimaterial by digital photoelasticity

M Ravichandran and **K Ramesh***
Department of Applied Mechanics, Indian Institute of Technology, Madras, India

The manuscript was received on 23 March 2004 and was accepted after revision for publication on 11 January 2005.

DOI: 10.1243/030932405X16034

Abstract: Photoelastic evaluation of the stress intensity factor (SIF) for a crack in a bimaterial tangential to the interface is hitherto confined to the use of only a singular stress field equation. In this paper, the multi-parameter stress field equations of Deng are simplified for use by experimentalists to evaluate the stress field parameters by digital photoelasticity using an overdeterministic least-squares technique. A bimaterial Brazilian disc with a central interface crack is selected as the model for study as different mode mixities could be easily simulated by changing the crack orientation angle. The use of SIF evaluation based on a singular stress field equation is found to be inadequate for the problems considered. On the other hand, the use of a multi-parameter stress field equation is quite successful in evaluating the stress field for various mode mixities and for two values of bimaterial constant. It is shown that the new procedure allows data collection from a larger zone, which helps to simplify data collection from experiments.

Keywords: interface crack, bimaterial, stress intensity factor (SIF), multi-parameter stress field equation, photoelasticity

1 INTRODUCTION

The plane problem of a crack lying along the interface of two dissimilar media in linear elasticity is one of great importance. The solution to such a problem could find application in the study of geological investigations dealing with fault lines along the interface between two layers of rock strata, the study of welded joints in which two dissimilar metallic materials are welded together with flaws or cracks developed along the original weld line owing to faulty joining techniques, the study of debonding of fibre-reinforced composites, etc. Williams [**1**] in 1959 formulated a bimaterial interface crack problem using the eigenfunction approach. He considered only the first eigenvalue in the sets of solution obtained and observed an oscillatory behaviour of the stresses when the crack tip is approached ($r \to 0$). He also observed that the oscillatory behaviour of the stresses is confined quite close to the base of the crack. The observations by Williams have been verified by Erdogan [**2**] and he noted that the oscillatory region is of the order of 10^{-6} of the crack length. The oscillatory character of the stresses implies interpenetration of the points on the crack surfaces as $r \to 0$. This does not arise in reality, as the crack tip cannot occupy two different materials at the same time. Several models have been proposed to handle the oscillatory character of stresses at the crack tip analytically [**3**]. The current understanding is that, although the elastic solution is wrong in detail on the scale of the contact zone, the models do nevertheless provide a proper characterizing parameter for the near-tip stress field. Hence, further discussion on the oscillatory character is beyond the purview of this paper.

In the case of a crack in a homogeneous medium, the stress field near the crack tip could be identified separately for mode-I (opening mode) and mode-II (shearing mode) loading and the corresponding stress intensity factors (SIFs) are labelled K_{I} and K_{II}. In the case of an interface crack in a bimaterial joint, the tensile and shear effects near the crack tip

*Corresponding author: Department of Applied Mechanics, Indian Institute of Technology, Madras, 600 036, India. email: kramesh@iitm.ac.in

are intrinsically inseparable and the SIF is usually expressed as a complex number. Various definitions of SIF are reported in the literature. The basic definition of the SIF has units of MPa $m^{1/2}$ $m^{-i\varepsilon}$ (ε is a bimaterial constant defined in section 2.1), which is inconvenient to use.

There are only limited studies on the photoelastic evaluation of the SIF for an interfacial crack in a bimaterial. Lu and Chiang [**4**] used the singular stress field equation in 1993 and incorporated a two-point approach for the evaluation of the complex stress intensity factor. Soh [**5**] in 1999 used a different definition of SIF from that used by Lu and Chiang and proposed SIF evaluation in a least-squares sense by taking a large number of points from the fringe contours. Although this technique attempts the use of field information of photoelastic fringes, the governing equation is still the singular stress field equation. Further, neither Lu and Chiang nor Soh made an attempt to reconstruct the isochromatics from their experimental results to verify the correctness of their solution.

For the problem of cracks in homogeneous solids, it is well documented that the use of singular solution to model the near-tip stress field is inadequate. The use of a multi-parameter solution to evaluate the SIF is well established [**6**]. Unlike the situation for the homogeneous case, in a bimaterial interface crack problem, the need for higher-order terms was not felt until 1987. In 1987, Symington [**7**] focused on the need for at least the constant stress term σ_{0x} as in the homogeneous case. Symington pointed out that the eigenvalues of Williams' solution can also have integer values which had been ignored by earlier researchers and he showed that the existence of a constant stress term for the bimaterial crack problem could be obtained from Williams' original solution. Using an analytic function formulation, Rice [**8**] in 1988 gave the form of series solution that includes integer order terms. Although the general form of stress field in a series form was presented by Rice, no explicit solution of the stress field in terms of r and θ was reported by him. Deng [**9**] reported in 1993 another form of the stress field equation in Cartesian coordinates. Although the form of equations given by Deng is simpler than that stated by Rice [**8**], still it is not in a form that could be directly used for numerical computations.

In this paper, the simplified form of multi-parameter equations used by Rice and Deng are presented. The stress field equations of Deng are modified so that the SIF has units of MPa $m^{1/2}$. Following the approach of Ramesh *et al.* [**6**], using the modified stress field equations of Deng, an over-deterministic least-squares approach is proposed for evaluating the stress field parameters. The methodology thus developed is applied for evaluating the stress field parameters in the vicinity of a central crack in a bimaterial Brazilian disc for different crack orientations and for two values of bimaterial constant. The required data for various problems considered are collected using digital photoelastic techniques such as fringe multiplication and fringe thinning. The isochromatic fringe patterns are reconstructed to verify the experimental solution. For completeness, the developments in the stress field equation starting from the singular solution and various definitions of the SIF are briefly summarized.

2 NEAR-TIP STRESS FIELD EQUATIONS IN THE NEIGHBOURHOOD OF AN INTERFACE CRACK IN BIMATERIAL JOINTS

2.1 Singular term stress field equations (very-near-tip field equations)

Figure 1 shows the immediate neighbourhood of an interface crack tangential to a bimaterial joint. The far-field loading is considered to be general, consisting of both normal and shear components. Let material 1 with elastic constants E_1 and ν_1 and material 2 with elastic constants E_2 and ν_2 occupy the upper and lower half-planes respectively, and let (x, y) be the global Cartesian coordinates. The early development of the solution to the bimaterial interface crack problem focused only on the singular terms. Such a solution can be termed the very-near-tip stress field equation. The basic singular stress

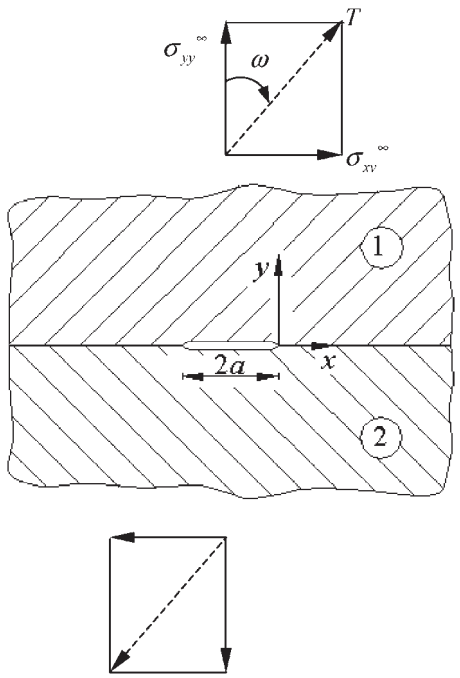

Fig. 1 Remote tension and shear loading of an interface crack

field equations obtained by Rice and Sih [**10**] are

$$(\sigma_{rr})_1 = \frac{k_1}{2\sqrt{2r}}\left\{e^{-\varepsilon(\pi-\theta)}\left[3\cos\left(\frac{\theta}{2}+\varepsilon\ln r\right)+2\varepsilon\sin\theta\cos\left(\frac{\theta}{2}-\varepsilon\ln r\right)-\sin\theta\sin\left(\frac{\theta}{2}-\varepsilon\ln r\right)\right]\right.$$
$$\left.-e^{\varepsilon(\pi-\theta)}\cos\left(\frac{3\theta}{2}+\varepsilon\ln r\right)\right\}$$
$$-\frac{k_2}{2\sqrt{2r}}\left\{e^{-\varepsilon(\pi-\theta)}\left[3\sin\left(\frac{\theta}{2}+\varepsilon\ln r\right)-2\varepsilon\sin\theta\sin\left(\frac{\theta}{2}-\varepsilon\ln r\right)-\sin\theta\cos\left(\frac{\theta}{2}-\varepsilon\ln r\right)\right]\right.$$
$$\left.-e^{\varepsilon(\pi-\theta)}\sin\left(\frac{3\theta}{2}+\varepsilon\ln r\right)\right\} \tag{1a}$$

$$(\sigma_{\theta\theta})_1 = \frac{k_1}{2\sqrt{2r}}\left\{e^{-\varepsilon(\pi-\theta)}\left[\cos\left(\frac{\theta}{2}+\varepsilon\ln r\right)-2\varepsilon\sin\theta\cos\left(\frac{\theta}{2}-\varepsilon\ln r\right)+\sin\theta\sin\left(\frac{\theta}{2}-\varepsilon\ln r\right)\right]\right.$$
$$\left.+e^{\varepsilon(\pi-\theta)}\cos\left(\frac{3\theta}{2}+\varepsilon\ln r\right)\right\}$$
$$-\frac{k_2}{2\sqrt{2r}}\left\{e^{-\varepsilon(\pi-\theta)}\left[\sin\left(\frac{\theta}{2}+\varepsilon\ln r\right)+2\varepsilon\sin\theta\sin\left(\frac{\theta}{2}-\varepsilon\ln r\right)+\sin\theta\cos\left(\frac{\theta}{2}-\varepsilon\ln r\right)\right]\right.$$
$$\left.+e^{\varepsilon(\pi-\theta)}\sin\left(\frac{3\theta}{2}+\varepsilon\ln r\right)\right\} \tag{1b}$$

$$(\tau_{r\theta})_1 = \frac{k_1}{2\sqrt{2r}}\left\{e^{-\varepsilon(\pi-\theta)}\left[\sin\left(\frac{\theta}{2}+\varepsilon\ln r\right)-2\varepsilon\sin\theta\sin\left(\frac{\theta}{2}-\varepsilon\ln r\right)-\sin\theta\cos\left(\frac{\theta}{2}-\varepsilon\ln r\right)\right]\right.$$
$$\left.+e^{\varepsilon(\pi-\theta)}\sin\left(\frac{3\theta}{2}+\varepsilon\ln r\right)\right\}$$
$$-\frac{k_2}{2\sqrt{2r}}\left\{e^{-\varepsilon(\pi-\theta)}\left[-\cos\left(\frac{\theta}{2}+\varepsilon\ln r\right)-2\varepsilon\sin\theta\cos\left(\frac{\theta}{2}-\varepsilon\ln r\right)+\sin\theta\sin\left(\frac{\theta}{2}-\varepsilon\ln r\right)\right]\right.$$
$$\left.-e^{\varepsilon(\pi-\theta)}\cos\left(\frac{3\theta}{2}+\varepsilon\ln r\right)\right\} \tag{1c}$$

where k_1 and k_2 are the stress intensity factors and ε is the bimaterial constant related to the elastic constants of materials 1 and 2 as

$$\varepsilon = \frac{1}{2\pi}\ln\left(\frac{G_2\kappa_1+G_1}{G_1\kappa_2+G_2}\right) \tag{2}$$

where G_j is the shear modulus, $\kappa_j = (3-\nu_j)/(1+\nu_j)$ for plane stress and $3-4\nu_j$ for plane strain $(j=1,2)$.

2.2 Definitions of the stress intensity factor

Various definitions of the SIF exist in the bimaterial literature. The tractions at a distance r ahead of the crack tip are obtained from equation (1) by putting $\theta = 0$ to give

$$(\sigma_{\theta\theta}+\mathrm{i}\tau_{r\theta})_{\theta=0} = \frac{k_1+\mathrm{i}k_2}{2\sqrt{2r}}r^{\mathrm{i}\varepsilon}(e^{-\varepsilon\pi}+e^{\varepsilon\pi})$$
$$= \frac{K}{\sqrt{2\pi r}}r^{\mathrm{i}\varepsilon} \tag{3}$$

where

$$K = K_1+\mathrm{i}K_2 = (k_1+\mathrm{i}k_2)\sqrt{\pi}\cosh(\pi\varepsilon) \tag{4}$$

Dimensional considerations dictate that K must be of the form [**11**]

$$K = K_1+\mathrm{i}K_2 = (\text{applied stress})\times(\sqrt{L}L^{-\mathrm{i}\varepsilon})f \tag{5}$$

where L is a characteristic length. The units of k_j or K_i $(i=1,2)$ for the bimaterial case is $\mathrm{MPa\,m^{1/2}\,m^{-i\varepsilon}}$. This is due to the presence of the characteristic length L that appears as $L^{-\mathrm{i}\varepsilon}$ in the SIF definition. To make the units of the SIF of the bimaterial interface crack similar to that of the homogeneous crack namely, $\mathrm{MPa\,m^{1/2}}$, two approaches have been reported. One is to include $L^{-\mathrm{i}\varepsilon}$ in the angular distribution function of the field solution given in equation (1). This was proposed by Shih and Asaro [**12**] and used by Soh [**5**]. The other proposed by Rice [**8**], is to multiply by an additional phase term $\hat{r}^{\mathrm{i}\varepsilon}$ instead of removing the phase term $L^{-\mathrm{i}\varepsilon}$. With these changes, SIFs are termed K_{I} and K_{II} instead of k_1 and k_2 or K_1

and K_2. It should be noted that, when the SIF subscript is in Roman numerals its units are MPa m$^{1/2}$. Although the units of SIF are the same as for the homogeneous case, their interpretation is quite different [**10**]. The multiplication of $\hat{r}^{i\varepsilon}$ proposed by Rice is simply the use of another characteristic length in order to obtain convenient units for the SIF and the later literature variously referred to it simply as $L^{i\varepsilon}$ or $\hat{L}^{i\varepsilon}$. Wang and Suo [**13**] reported that it does not matter whether $\hat{L}$ is set equal to 1 μm, 0.1 mm, or 5 cm so long as a fixed length is chosen in reporting SIF data.

2.3 Multi-parameter stress field equations

Rice [**8**] was the first to report a complete form of stress field in polar coordinates based on the analytic function method. The solution obtained is not in a form that could be used by experimentalists. Appendix 2 gives the simplified stress field equations based on Rice's work. The details of the simplification can be found in reference [**14**]. Although, in 1993, Deng [**9**] reported another form of multi-parameter stress field equations for an interface crack in a homogeneous bimaterial, the paper has remained obscure for researchers dealing with the interface crack of homogeneous materials for a long time. The equation reported by Deng is found to be much simpler to handle than that of Rice in the present study. The Cartesian stress components of the stress field obtained by Deng [**9**] are reported as

$$\sigma(r,\theta) = \sum_{n=0}^{\infty} r^{(n-1)/2} \times \left[\frac{\mathrm{Re}(k_n r^{i\varepsilon})}{\sqrt{2\pi}} \hat{\sigma}_n^{\mathrm{I}}(\theta) + \frac{\mathrm{Im}(k_n r^{i\varepsilon})}{\sqrt{2\pi}} \hat{\sigma}_n^{\mathrm{II}}(\theta) \right] \quad (6)$$

where k_n is a complex coefficient given by $k_{\mathrm{I}n} + ik_{\mathrm{II}n}$, ε is the bimaterial constant (equal to zero when $n = 1, 3, 5, \ldots$), and $\hat{\sigma}_n^{\mathrm{I}}(\theta)$ and $\hat{\sigma}_n^{\mathrm{II}}(\theta)$ are the angular functions given below. The expressions for the angular functions for the top half-plane when $n = 0, 2, 4, \ldots$ are given by

$$\begin{Bmatrix} \hat{\sigma}_{xxn}^{\mathrm{I}}(\theta) \\ \hat{\sigma}_{yyn}^{\mathrm{I}}(\theta) \\ \hat{\sigma}_{xyn}^{\mathrm{I}}(\theta) \end{Bmatrix} = \frac{1}{\cosh \pi\varepsilon} \times \begin{Bmatrix} -\{\sinh[\varepsilon(\pi-\theta)] - \mathrm{e}^{-\varepsilon(\pi-\theta)}\} \cos\left(\frac{n-1}{2}\theta\right) - \frac{1}{2}\mathrm{e}^{-\varepsilon(\pi-\theta)} \sin\theta \left[(n-1)\sin\left(\frac{n-3}{2}\theta\right) - 2\varepsilon\cos\left(\frac{n-3}{2}\theta\right)\right] \\ \{\sinh[\varepsilon(\pi-\theta)] + \mathrm{e}^{-\varepsilon(\pi-\theta)}\} \cos\left(\frac{n-1}{2}\theta\right) + \frac{1}{2}\mathrm{e}^{-\varepsilon(\pi-\theta)} \sin\theta \left[(n-1)\sin\left(\frac{n-3}{2}\theta\right) - 2\varepsilon\cos\left(\frac{n-3}{2}\theta\right)\right] \\ \sinh[\varepsilon(\pi-\theta)] \sin\left(\frac{n-1}{2}\theta\right) - \frac{1}{2}\mathrm{e}^{-\varepsilon(\pi-\theta)} \sin\theta \left[(n-1)\cos\left(\frac{n-3}{2}\theta\right) + 2\varepsilon\sin\left(\frac{n-3}{2}\theta\right)\right] \end{Bmatrix} \quad (7a)$$

$$\begin{Bmatrix} \hat{\sigma}_{xxn}^{\mathrm{II}}(\theta) \\ \hat{\sigma}_{yyn}^{\mathrm{II}}(\theta) \\ \hat{\sigma}_{xyn}^{\mathrm{II}}(\theta) \end{Bmatrix} = \frac{1}{\cosh(\pi\varepsilon)} \times \begin{Bmatrix} \{\cosh[\varepsilon(\pi-\theta)] + \mathrm{e}^{-\varepsilon(\pi-\theta)}\} \sin\left(\frac{n-1}{2}\theta\right) + \frac{1}{2}\mathrm{e}^{-\varepsilon(\pi-\theta)} \sin\theta \left[(n-1)\cos\left(\frac{n-3}{2}\theta\right) + 2\varepsilon\sin\left(\frac{n-3}{2}\theta\right)\right] \\ -\{\cosh[\varepsilon(\pi-\theta)] - \mathrm{e}^{-\varepsilon(\pi-\theta)}\} \sin\left(\frac{n-1}{2}\theta\right) - \frac{1}{2}\mathrm{e}^{-\varepsilon(\pi-\theta)} \sin\theta \left[(n-1)\cos\left(\frac{n-3}{2}\theta\right) + 2\varepsilon\sin\left(\frac{n-3}{2}\theta\right)\right] \\ \cosh[\varepsilon(\pi-\theta)] \cos\left(\frac{n-1}{2}\theta\right) - \frac{1}{2}\mathrm{e}^{-\varepsilon(\pi-\theta)} \sin\theta \left[(n-1)\sin\left(\frac{n-3}{2}\theta\right) - 2\varepsilon\cos\left(\frac{n-3}{2}\theta\right)\right] \end{Bmatrix} \quad (7b)$$

and when $n = 1, 3, 5, \ldots$ the angular functions are given by

$$\begin{Bmatrix} \hat{\sigma}^{\mathrm{I}}_{xxn}(\theta) \\ \hat{\sigma}^{\mathrm{I}}_{yyn}(\theta) \\ \hat{\sigma}^{\mathrm{I}}_{xyn}(\theta) \end{Bmatrix} = \frac{1}{1+w} \begin{Bmatrix} 4\cos\left(\dfrac{n-1}{2}\theta\right) - (n-1)\sin\theta\sin\left(\dfrac{n-3}{2}\theta\right) \\ (n-1)\sin\theta\sin\left(\dfrac{n-3}{2}\theta\right) \\ -2\sin\left(\dfrac{n-1}{2}\theta\right) - (n-1)\sin\theta\cos\left(\dfrac{n-3}{2}\theta\right) \end{Bmatrix} \tag{7c}$$

$$\begin{Bmatrix} \hat{\sigma}^{\mathrm{II}}_{xxn}(\theta) \\ \hat{\sigma}^{\mathrm{II}}_{yyn}(\theta) \\ \hat{\sigma}^{\mathrm{II}}_{xyn}(\theta) \end{Bmatrix} = \frac{1}{1+w} \begin{Bmatrix} 2\sin\left(\dfrac{n-1}{2}\theta\right) + (n-1)\sin\theta\cos\left(\dfrac{n-3}{2}\theta\right) \\ 2\sin\left(\dfrac{n-1}{2}\theta\right) - (n-1)\sin\theta\cos\left(\dfrac{n-3}{2}\theta\right) \\ -(n-1)\sin\theta\sin\left(\dfrac{n-3}{2}\theta\right) \end{Bmatrix} \tag{7d}$$

where

$$w = \frac{(1+\kappa_1)G_2}{(1+\kappa_2)G_1}$$

Although Deng reported the SIF as $k_{\mathrm{I}0} + \mathrm{i}k_{\mathrm{II}0}$, it is actually K_1 and K_2 (as in section 2.2) with units of $\mathrm{MPa\,m^{1/2}\,m^{-i\varepsilon}}$. The interest here is to obtain K_{I} and K_{II}. Following the work of Soh [**5**], the length quantity $L^{-\mathrm{i}\varepsilon}$ is included in the angular function of the stress field. The Cartesian stress components are

$$\begin{Bmatrix} (\sigma_{xx})_1 \\ (\sigma_{yy})_1 \\ (\tau_{xy})_1 \end{Bmatrix} = \sum_{n=0,2,4}^{\infty} \frac{K_{\mathrm{I}n}}{Q} r^{(n-1)/2} \begin{Bmatrix} S\left\{3\cos\left[\dfrac{n-1}{2}\theta - \varepsilon\ln\left(\dfrac{r}{L}\right)\right] - (n-1)\sin\theta\sin\left[\dfrac{n-3}{2}\theta - \varepsilon\ln\left(\dfrac{r}{L}\right)\right]\right. \\ S\left\{\cos\left[\dfrac{n-1}{2}\theta - \varepsilon\ln\left(\dfrac{r}{L}\right)\right] + (n-1)\sin\theta\sin\left[\dfrac{n-3}{2}\theta - \varepsilon\ln\left(\dfrac{r}{L}\right)\right]\right. \\ S\left\{-\sin\left[\dfrac{n-1}{2}\theta - \varepsilon\ln\left(\dfrac{r}{L}\right)\right] - (n-1)\sin\theta\cos\left[\dfrac{n-3}{2}\theta - \varepsilon\ln\left(\dfrac{r}{L}\right)\right]\right. \end{Bmatrix}$$

$$\begin{Bmatrix} \left. +2\varepsilon\sin\theta\cos\left[\dfrac{n-3}{2}\theta - \varepsilon\ln\left(\dfrac{r}{L}\right)\right]\right\} - \dfrac{1}{S}\cos\left[\dfrac{n-1}{2}\theta + \varepsilon\ln\left(\dfrac{r}{L}\right)\right] \\ \left. -2\varepsilon\sin\theta\cos\left[\dfrac{n-3}{2}\theta - \varepsilon\ln\left(\dfrac{r}{L}\right)\right]\right\} + \dfrac{1}{S}\cos\left[\dfrac{n-1}{2}\theta + \varepsilon\ln\left(\dfrac{r}{L}\right)\right] \\ \left. -2\varepsilon\sin\theta\sin\left[\dfrac{n-3}{2}\theta - \varepsilon\ln\left(\dfrac{r}{L}\right)\right]\right\} + \dfrac{1}{S}\sin\left[\dfrac{n-1}{2}\theta + \varepsilon\ln\left(\dfrac{r}{L}\right)\right] \end{Bmatrix}$$

$$+ \sum_{n=1,3,5}^{\infty} \frac{K_{\mathrm{I}n}}{R} r^{(n-1)/2} \begin{Bmatrix} 4\cos\left(\dfrac{n-1}{2}\theta\right) - (n-1)\sin\theta\sin\left(\dfrac{n-3}{2}\theta\right) \\ (n-1)\sin\theta\sin\left(\dfrac{n-3}{2}\theta\right) \\ -2\sin\left(\dfrac{n-1}{2}\theta\right) - (n-1)\sin\theta\cos\left(\dfrac{n-3}{2}\theta\right) \end{Bmatrix}$$

$$+\sum_{n=0,2,4}^{\infty}\frac{K_{\mathrm{II}n}}{Q}r^{(n-1)/2}\left\{\begin{array}{l} S\left\{3\sin\left[\dfrac{n-1}{2}\theta-\varepsilon\ln\left(\dfrac{r}{L}\right)\right]+(n-1)\sin\theta\cos\left[\dfrac{n-3}{2}\theta-\varepsilon\ln\left(\dfrac{r}{L}\right)\right]\right. \\ S\left\{\sin\left[\dfrac{n-1}{2}\theta-\varepsilon\ln\left(\dfrac{r}{L}\right)\right]-(n-1)\sin\theta\cos\left[\dfrac{n-3}{2}\theta-\varepsilon\ln\left(\dfrac{r}{L}\right)\right]\right. \\ S\left\{\cos\left[\dfrac{n-1}{2}\theta-\varepsilon\ln\left(\dfrac{r}{L}\right)\right]-(n-1)\sin\theta\sin\left[\dfrac{n-3}{2}\theta-\varepsilon\ln\left(\dfrac{r}{L}\right)\right]\right. \end{array}\right.$$

$$\left.\begin{array}{l} \left.+2\varepsilon\sin\theta\sin\left[\dfrac{n-3}{2}\theta-\varepsilon\ln\left(\dfrac{r}{L}\right)\right]\right\}+\dfrac{1}{S}\sin\left[\dfrac{n-1}{2}\theta+\varepsilon\ln\left(\dfrac{r}{L}\right)\right] \\ \left.-2\varepsilon\sin\theta\sin\left[\dfrac{n-3}{2}\theta-\varepsilon\ln\left(\dfrac{r}{L}\right)\right]\right\}-\dfrac{1}{S}\sin\left[\dfrac{n-1}{2}\theta+\varepsilon\ln\left(\dfrac{r}{L}\right)\right] \\ \left.+2\varepsilon\sin\theta\cos\left[\dfrac{n-3}{2}\theta-\varepsilon\ln\left(\dfrac{r}{L}\right)\right]\right\}+\dfrac{1}{S}\cos\left[\dfrac{n-1}{2}\theta+\varepsilon\ln\left(\dfrac{r}{L}\right)\right] \end{array}\right\}$$

$$+\sum_{n=1,3,5}^{\infty}\frac{K_{\mathrm{II}n}}{R}r^{(n-1)/2}\left\{\begin{array}{c} 2\sin\left(\dfrac{n-1}{2}\theta\right)+(n-1)\sin\theta\cos\left(\dfrac{n-3}{2}\theta\right) \\ 2\sin\left(\dfrac{n-1}{2}\theta\right)-(n-1)\sin\theta\cos\left(\dfrac{n-3}{2}\theta\right) \\ -(n-1)\sin\theta\sin\left(\dfrac{n-3}{2}\theta\right) \end{array}\right\} \tag{8}$$

where

$$Q=2\sqrt{2\pi}\cosh(\pi\varepsilon),\qquad R=\sqrt{2\pi}(1+w)$$
$$S=\mathrm{e}^{-\varepsilon(\pi-\theta)}$$

The stress field expressions for the bottom half-plane can be obtained simply by changing $\mathrm{e}^{\varepsilon\pi}$ to $\mathrm{e}^{-\varepsilon\pi}$, $\mathrm{e}^{-\varepsilon\pi}$ to $\mathrm{e}^{\varepsilon\pi}$, and w to $1/w$. It was verified numerically in reference [**14**] that, when $\varepsilon=0$, equation (8) reduces to the multi-parameter equations of Atluri and Kobayashi [**15**] for the homogeneous problem. When equation (8) is transformed into polar coordinates, the first term of the equation ($n=0$) is the same as equation (1) [**14**].

3 EVALUATION OF THE STRESS FIELD PARAMETERS USING THE LEAST-SQUARES METHOD

The well-known stress-optic law of photoelasticity relates the fringe order N and difference in principal stress as

$$\sigma_1-\sigma_2=\frac{NF_\sigma}{h} \tag{9}$$

where F_σ is the material stress fringe value of the photoelastic model and h is the thickness of the photoelastic model. Expressing the principal stresses in terms of stress components, a least-squares function g is defined for the mth data point as

$$g_m=\left(\frac{\sigma_{xx}-\sigma_{yy}}{2}\right)_m^2+(\tau_{xy})_m^2-\left(\frac{N_mF_\sigma}{2h}\right)^2 \tag{10}$$

Equation (10) is non-linear in terms of the unknown stress field parameters $K_{\mathrm{I}1}$, $K_{\mathrm{I}2}$, …, $K_{\mathrm{I}k}$ and $K_{\mathrm{II}1}$, $K_{\mathrm{II}2}$, …, $K_{\mathrm{II}l}$, where k is the number of K_{I} parameters and l is the number of K_{II} parameters being considered. Apart from these unknowns, *a priori* the values of k and l are also not known and they have to be found as part of the solution. If initial estimates are made for $K_{\mathrm{I}n}$ and $K_{\mathrm{II}n}$ and substituted in the above equation, it is possible that $g_m\neq 0$ since the estimates may not be accurate. To correct the estimates, a series of iterative equations based on a Taylor series expansion of g_m are written as

$$\begin{aligned}(g_m)_{i+1}=(g_m)_i&+\left(\frac{\partial g_m}{\partial K_{\mathrm{I}1}}\right)_i(\Delta K_{\mathrm{I}1})_i+\left(\frac{\partial g_m}{\partial K_{\mathrm{I}2}}\right)_i(\Delta K_{\mathrm{I}2})_i\\&+\cdots+\left(\frac{\partial g_m}{\partial K_{\mathrm{I}k}}\right)_i(\Delta K_{\mathrm{I}k})_i+\left(\frac{\partial g_m}{\partial K_{\mathrm{II}1}}\right)_i(\Delta K_{\mathrm{II}1})_i\\&+\left(\frac{\partial g_m}{\partial K_{\mathrm{II}2}}\right)_i(\Delta K_{\mathrm{II}2})_i+\cdots+\left(\frac{\partial g_m}{\partial K_{\mathrm{II}l}}\right)_i(\Delta K_{\mathrm{II}l})_i\end{aligned} \tag{11}$$

The corrections of the unknown parameters $\Delta K_{\mathrm{I}1}$, $\Delta K_{\mathrm{I}2}$, …, etc., are determined such that $(g_m)_{i+1}=0$. In forming equation (11) it is necessary to calculate $(\partial g_m/\partial K_{\mathrm{I}1})$, $(\partial g_m/\partial K_{\mathrm{I}2})$, …, etc., and at first it appears

that this may be difficult to achieve in closed form. However, it can be determined very easily. A typical derivative for the mth data point with respect to $K_{\mathrm{I}n}$ is obtained by taking the derivative of equation (10) according to

$$\frac{\partial g_m}{\partial K_{\mathrm{I}n}} = \frac{1}{2}(\sigma_x - \sigma_y)_m \left(\frac{\partial \sigma_x}{\partial K_{\mathrm{I}n}} - \frac{\partial \sigma_y}{\partial K_{\mathrm{I}n}} \right)_m + 2\left(\tau_{xy} \frac{\partial \tau_{xy}}{\partial K_{\mathrm{I}n}} \right)_m \tag{12}$$

Since $K_{\mathrm{I}n}$ is a linear coefficient in the stress field equation given in equation (8), the terms $(\partial\sigma_x/\partial K_{\mathrm{I}n})$, etc., in equation (12) are simply obtained from equation (8) as, when $n = 0, 2, 4, \ldots$,

$$\begin{Bmatrix} \dfrac{\partial \sigma_{xx}}{\partial K_{\mathrm{I}n}} \\ \dfrac{\partial \sigma_{yy}}{\partial K_{\mathrm{I}n}} \\ \dfrac{\partial \tau_{xy}}{\partial K_{\mathrm{I}n}} \end{Bmatrix} = \frac{r^{(n-1)/2}}{Q} \begin{Bmatrix} S\left\{ 3\cos\left[\dfrac{n-1}{2}\theta - \varepsilon \ln\left(\dfrac{r}{L} \right) \right] - (n-1)\sin\theta \sin\left[\dfrac{n-3}{2}\theta - \varepsilon \ln\left(\dfrac{r}{L} \right) \right] \right. \\ S\left\{ \cos\left[\dfrac{n-1}{2}\theta - \varepsilon \ln\left(\dfrac{r}{L} \right) \right] + (n-1)\sin\theta \sin\left[\dfrac{n-3}{2}\theta - \varepsilon \ln\left(\dfrac{r}{L} \right) \right] \right. \\ S\left\{ -\sin\left[\dfrac{n-1}{2}\theta - \varepsilon \ln\left(\dfrac{r}{L} \right) \right] - (n-1)\sin\theta \cos\left[\dfrac{n-3}{2}\theta - \varepsilon \ln\left(\dfrac{r}{L} \right) \right] \right. \end{Bmatrix}$$

$$\begin{Bmatrix} +2\varepsilon \sin\theta \cos\left[\dfrac{n-3}{2}\theta - \varepsilon \ln\left(\dfrac{r}{L} \right) \right] \Big\} - \dfrac{1}{S}\cos\left[\dfrac{n-1}{2}\theta + \varepsilon \ln\left(\dfrac{r}{L} \right) \right] \\ -2\varepsilon \sin\theta \cos\left[\dfrac{n-3}{2}\theta - \varepsilon \ln\left(\dfrac{r}{L} \right) \right] \Big\} + \dfrac{1}{S}\cos\left[\dfrac{n-1}{2}\theta + \varepsilon \ln\left(\dfrac{r}{L} \right) \right] \\ -2\varepsilon \sin\theta \sin\left[\dfrac{n-3}{2}\theta - \varepsilon \ln\left(\dfrac{r}{L} \right) \right] \Big\} + \dfrac{1}{S}\sin\left[\dfrac{n-1}{2}\theta + \varepsilon \ln\left(\dfrac{r}{L} \right) \right] \end{Bmatrix} \tag{13a}$$

and, when $n = 1, 3, 5, \ldots$,

$$\begin{Bmatrix} \dfrac{\partial \sigma_{xx}}{\partial K_{\mathrm{I}n}} \\ \dfrac{\partial \sigma_{yy}}{\partial K_{\mathrm{I}n}} \\ \dfrac{\partial \tau_{xy}}{\partial K_{\mathrm{I}n}} \end{Bmatrix} = \frac{r^{(n-1)/2}}{R} \begin{Bmatrix} 4\cos\left(\dfrac{n-1}{2}\theta \right) - (n-1)\sin\theta \sin\left(\dfrac{n-3}{2}\theta \right) \\ (n-1)\sin\theta \sin\left(\dfrac{n-3}{2}\theta \right) \\ -2\sin\left(\dfrac{n-1}{2}\theta \right) - (n-1)\sin\theta \cos\left(\dfrac{n-3}{2}\theta \right) \end{Bmatrix} \tag{13b}$$

Similarly the derivative with respect to $K_{\mathrm{II}n}$ for the mth data point can be computed. A software has been implemented on the MFC environment in Visual C++ to evaluate the stress field parameters using up to eight terms of the multi-parameter stress field equation. Following the work of Soh [**5**], the characteristic length L is taken as the crack length $2a$ in the software. The software requires a data file containing the x and y coordinates and the corresponding fringe order as the input.

The iteration is stopped by using the criteria of fringe order error minimization. In this, using the newly calculated values of $(K_{\mathrm{I}})_{i+1}$ and $(K_{\mathrm{II}})_{i+1}$, the fringe orders corresponding to the selected data points are calculated theoretically during each iteration step. The convergence criteria are satisfied if

$$\frac{\sum |N_{\mathrm{theory}} - N_{\mathrm{exp}}|}{\text{total number of data points}} \leqslant \text{convergence error} \tag{14}$$

The best solution is obtained when the convergence error is less than 0.05 [**14**]. Using the parameters thus obtained, the program recalculates $\sigma_1 - \sigma_2$ values, and hence the fringe order at every point in the data field, which is used to reconstruct the stress field for comparison. The comparison is necessary to verify that the iteration scheme has indeed converged to the solution of the problem. Instances have been reported in the literature for cracks in homogeneous material for which, although the convergence is obtained, the solution is not correct as the reconstructed fringe field is different [**16**]!

4 EXPERIMENTAL VALIDATION

4.1 Choice of bimaterial specimen

Lu and Chiang [**4**] and Soh [**5**] used a rectangular bimaterial joint for their photoelastic tests. The problems that they studied were confined to predominantly mode-I loading. Further, they carefully chose their specimens so that a singular solution was valid for short cracks. In this paper, a bimaterial Brazilian disc

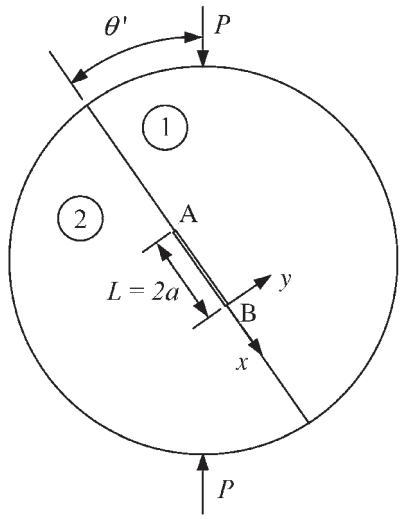

Fig. 2 Brazilian disc and coordinates

(Fig. 2) is used for photoelastic studies. A variety of mode mixities can be obtained easily in this specimen by changing the crack orientation angle with respect to the point of load application. In view of the easy control on the loading, the governing equations developed in section 2.3 could be verified for various mode mixities too.

4.2 Experimental procedure for making a bimaterial specimen

The simplest procedure for making a bimaterial joint is by joining two halves made from materials with the help of an adhesive, provided that the adhesive is made from either of the parent materials. If the adhesive is not one of the parent materials, the entire system becomes a trimaterial. In the bimaterial joints used in this study, epoxy is one of the parent materials and epoxy adhesive is used as a bonding medium. Table 1 summarizes the elastic and optical properties of the material combinations used.

Semicircular discs (of diameter 60 mm) of epoxy and the other material (PSM1 or mild steel as the case may be), which are needed for making a bimaterial joint, are machined initially. The residual stresses on the edges of halves are minimized by using a single-point cutting tool at a high speed. The bonding surfaces of the two halves are then roughened using 220-grit emery, and the surfaces are subsequently cleaned with laboratory-grade isopropyl alcohol. The adhesive is then prepared by mixing CY230 epoxy resin and HY951 hardener in the weight ratio 10:1. A thin Teflon layer (of thickness 0.075 mm) equal to a crack length of 19 mm is placed at the centre of the semicircular disc to assist the formation of an interface crack. Silicone grease is applied on the Teflon layer so that, after curing, it can be easily removed from the interface. The adhesive prepared is then applied on the surfaces and placed in a fixture arrangement. A light clamping pressure is applied from both ends of the fixture using springs, and the specimen is allowed to cure for 36 h. The Teflon layer is then removed from the joint and the excess portion of the bonding medium is removed by using water emery of 600 grit.

4.3 Use of fringe multiplication and fringe thinning in augmenting fringe data collection

One of the main difficulties encountered in experiments involving interface cracks was the lack of a sufficient number of fringes for analysis. Figures 3(a) and (b) show the closer views of dark-field and bright-field isochromatics grabbed using a monochrome camera. It can be seen from the figure that the fringes are not sufficient to collect the stress field information. In principle, the number of fringes seen in the experiment could be increased if the load is increased. However, if the load is increased, the model fractured in certain crack orientations. In view of this, the quantum of data that can be collected is limited. A solution to this problem is found by resorting to digital fringe multiplication. A simple digital subtraction of bright- and dark-field images could result in fringe multiplication by an order of two [**17**]. The resulting image is termed a *mixed-field image* and is shown in Fig. 3(c). The fringes are now sufficient to collect the stress field information.

Although the mixed-field image appears sharp in some zones, for data collection it is desirable to identify the skeleton for improved accuracy. A global fringe-thinning algorithm [**18, 19**] is used to identify the fringe skeleton. This algorithm is computationally fast and uses intensity information for the location of the fringe skeleton.

Table 1 Material properties (subscripts 1 and 2 refer to materials 1 and 2 respectively)

Bimaterial	E_1 (GPa)	ν_1	E_2 (GPa)	ν_2	$F_{\sigma 1}$ (N/mm fringe)	$F_{\sigma 2}$ (N/mm fringe)	ε
PSM1*–epoxy	2.5	0.38	3.3	0.33	7.00	13.44	0.01
Epoxy–mild steel	3.3	0.33	210	0.3	13.44	–	0.10

* Polycarbonate, Measurements Group Inc., USA.

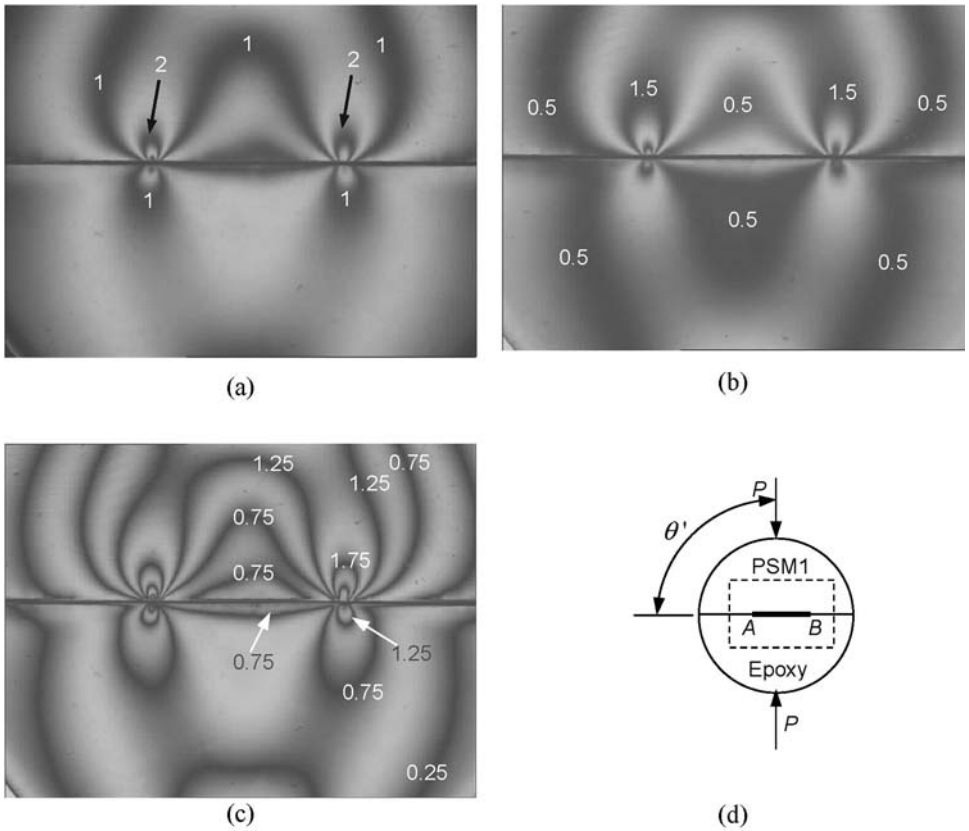

Fig. 3 Closer view [for the dash box shown in (d)] of isochromatics for a bimaterial Brazilian disc (PSM1–epoxy; $\varepsilon = 0.01$; $\theta' = 90^\circ$ (89.8°); $h = 5.6$ mm; load, 205 N; $F_{\sigma 1} = 7$ N/mm fringe; $F_{\sigma 2} = 13.44$ N/mm fringe): (a) dark field; (b) bright field; (c) mixed field

4.4 Evaluation of the stress intensity factors using the least-squares method

The least-squares procedure of SIF evaluation is illustrated in this section by considering the crack tip B of the bimaterial interface crack problem shown in Fig. 3(d). First, the data on the PSM1 side are taken for analysis. The fringe order and the corresponding positional coordinates at fringe locations are collected from the thinned mixed-field image. The data points are selected in such a way that, when plotted, they capture the basic geometric features of the fringe field. Since the number of parameters involved in characterizing the stress field are not known *a priori*, the iteration is started with two terms each of K_{I} and K_{II} series (Fig. 4). The solution thus obtained may not be quite comparable with the experimental fringes; the iteration is performed with a large convergence error (fringe order error minimization) of the order of 0.5.

Using the solution of the terms thus obtained as starting values, the number of terms in each series is increased by one. The convergence error to stop the iteration is reduced from what was obtained for the two-term solution and the iterative evaluation of the parameters is continued. The number of parameters is then increased by one and the iteration is continued with the increased number of terms until the convergence error obtained is of the order of 0.05. Table 2 summarizes the value of stress field parameters for the problem considered starting from two-term to five-term solutions. The convergence error obtained has reduced from 0.41 for a two-parameter (totally four) solution to 0.04 for a five-parameter (totally ten) solution. To appreciate the process of convergence visually, at each stage of the converged solution, the fringes are reconstructed with the specified number of parameters and data points are echoed back for comparison (Fig. 5). Inspection of Fig. 5 shows that the data points match well for a five-term solution compared with a two-term solution.

4.5 Discussion

It is clear from the analysis that, for the problem considered, a singular solution would not have been adequate to model the stress field. A recent reference [**20**] has emphasized the facts that the size of the singularity-dominated zone is problem dependent and that the data collection zone becomes exceedingly small in general. Further, for some problems,

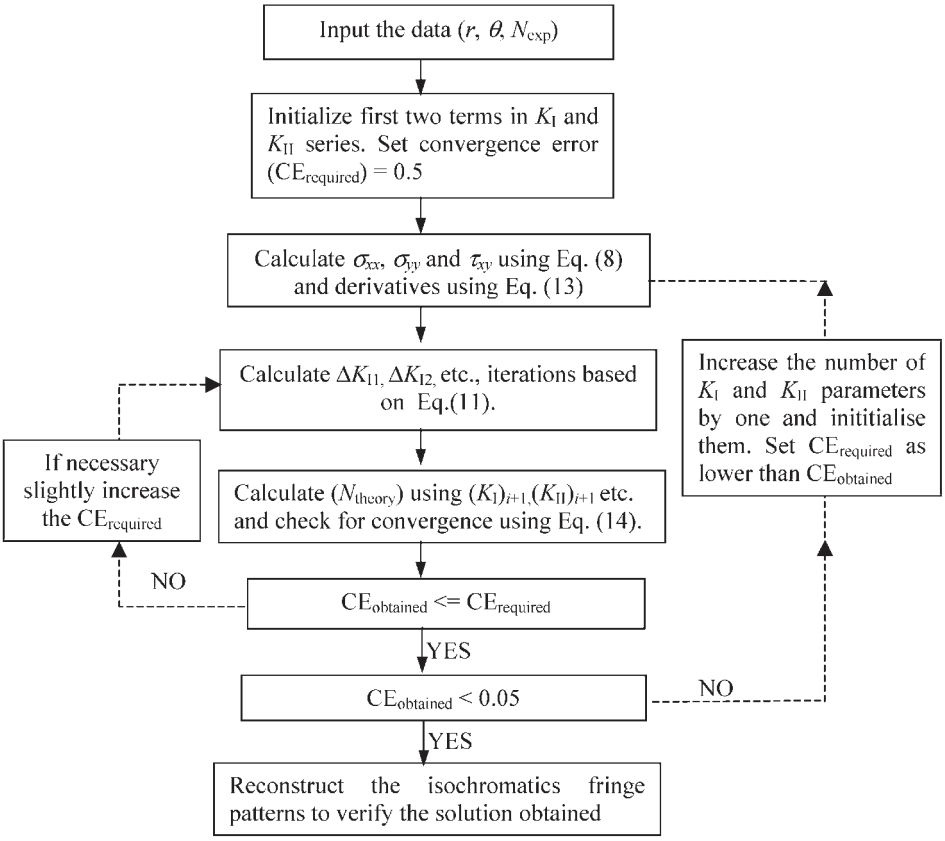

Fig. 4 Flow chart of least-squares evaluation of the multi-parameter stress field

collecting data even by fringe multiplication for employing the constant-radius method [**4**] is not possible and phase-shifting techniques had to be resorted to for data collection. The need to evaluate the stress field by a multi-parameter solution is clearly shown in reference [**20**] and the present work fulfils that requirement. Table 2 indicates that the range of data collection zone for the present methodology in terms of the r/a ratio is reasonable for convenient data collection from experiments.

Unlike other work on the photoelastic evaluation of the SIF [**4**, **5**], here the SIFs are also evaluated using the data points obtained from the material below the interface, i.e. epoxy in this case. The governing

Table 2 Summary of the stress field parameters evaluated from field data corresponding to PSM1 in the bimaterial Brazilian disc (PSM1–epoxy; $\varepsilon = 0.01$; $\theta' = 90^\circ$ (89.8°); $h = 5.6$ mm; load, 205 N; $F_{\sigma 1} = 7$ N/mm fringe)

	Two-term solution	Three-term solution	Four-term solution	Five-term solution
K_I (MPa m$^{1/2}$)	0.151	0.179	0.194	0.188
K_{II} (MPa m$^{1/2}$)	−0.041	−0.001	−0.034	−0.035
$\|K\|$ (MPa m$^{1/2}$)	0.156	0.179	0.197	0.191
K_{I1} (MPa mm$^{1/2}$)	4.7788	5.6582	6.1265	5.9503
K_{I2} (MPa)	−2.3686	−0.9200	−1.5234	−1.9790
K_{I3} (MPa mm$^{-1/2}$)		2.2984	−0.2048	1.6521
K_{I4} (MPa mm^{-1})			0.0259	0.3746
K_{I5} (MPa mm$^{-3/2}$)				−0.2069
K_{II1} (MPa mm$^{1/2}$)	−1.2870	−0.0403	−1.0779	−1.0913
K_{II2} (MPa)	0.0000	0.0000	0.0000	0.0000
K_{II3} (MPa mm$^{-1/2}$)		−0.6349	−0.0960	0.5413
K_{II4} (MPa mm^{-1})			0.0807	−0.9267
K_{II5} (MPa mm$^{-3/2}$)				−0.0129
Convergence error obtained	0.41	0.17	0.07	0.04
Data collection range	$(r/a)_{min}$	0.11	$(r/a)_{max}$	0.65

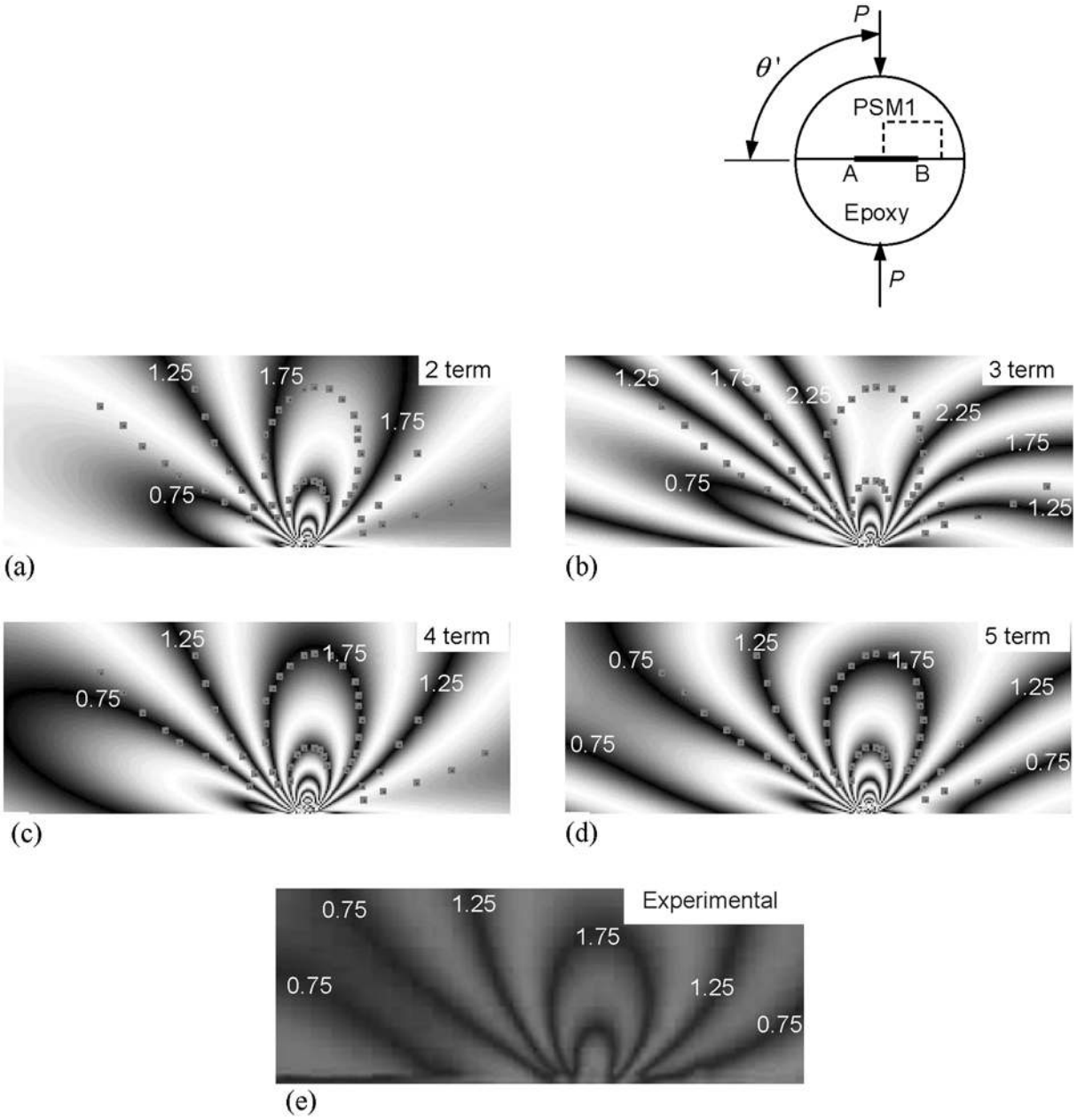

Fig. 5 (a)–(d) Theoretically reconstructed mixed field isochromatics with data points echoed using the experimentally obtained parameters for PSM1 of PSM1–epoxy ($\varepsilon = 0.01$; $\theta' = 90^\circ$ (89.8°); $h = 5.6$ mm; load, 205 N; $F_{\sigma 1} = 7.0$ N/mm fringe) and (e) experimental mixed field isochromatics

equation needs to be modified as mentioned in section 2.3. For this problem case, a six-term solution is found to be necessary (Table 3) and the reconstructed image for the six-parameter solution compares well with the experimental image (Fig. 6). Comparison of Tables 2 and 3 show that K_{I} and K_{II} obtained from each material side are comparable. The other terms of the series are different and capture the stress field information of the two materials appropriately. In view of the good comparison of theoretically simulated fringes with the experimental fringes, the validity of the multi-parameter stress field equation developed for both the material sides in section 2.3 is verified.

4.6 Evaluation of stress field parameters for various crack orientations and two bimaterial pairs

The procedure mentioned in section 3 is followed to obtain the stress field parameters for various crack orientations and for two bimaterial specimens having $\varepsilon = 0.01$ and 0.1 in the neighbourhood of crack tip B. The magnitude of the external loading is

Table 3 Summary of the stress field parameters evaluated from field data corresponding to epoxy in the bimaterial Brazilian disc (PSM1–epoxy; $\varepsilon = 0.01$, $\theta' = 90^\circ$ (89.8°); $h = 5.6$ mm; load, 205 N; $F_{\sigma 1} = 13.44$ N/mm fringe)

	Two-term solution	Three-term solution	Four-term solution	Five-term solution	Six-term solution
K_{I} (MPa m$^{1/2}$)	0.057	0.112	0.200	0.203	0.180
K_{II} (MPa m$^{1/2}$)	0.196	0.134	−0.002	0.011	0.028
$\lvert K\rvert$ (MPa m$^{1/2}$)	0.204	0.175	0.200	0.203	0.182
$K_{\mathrm{I}1}$ (MPa mm$^{1/2}$)	1.8070	3.5267	6.3270	6.4071	5.6509
$K_{\mathrm{I}2}$ (MPa)	−2.7643	−2.4583	−2.0559	−2.2102	−3.0864
$K_{\mathrm{I}3}$ (MPa mm$^{-1/2}$)		1.7155	2.1910	0.2156	1.5471
$K_{\mathrm{I}4}$ (MPa mm^{-1})			−0.0850	0.0709	0.4420
$K_{\mathrm{I}5}$ (MPa mm$^{-3/2}$)				−0.0042	−0.2902
$K_{\mathrm{I}6}$ (MPa mm^{-2})					0.0006
$K_{\mathrm{II}1}$ (MPa mm$^{1/2}$)	6.2136	4.2342	−0.0709	0.3353	0.9009
$K_{\mathrm{II}2}$ (MPa)	0.0000	0.0000	0.0000	0.0000	0.0000
$K_{\mathrm{II}3}$ (MPa mm$^{-1/2}$)		0.0646	0.9962	0.6755	−0.1248
$K_{\mathrm{II}4}$ (MPa mm^{-1})			−0.9377	−1.0147	−0.3322
$K_{\mathrm{II}5}$ (MPa mm$^{-3/2}$)				0.0561	0.1416
$K_{\mathrm{II}6}$ (MPa mm^{-2})					−0.0331
Convergence error obtained	0.36	0.24	0.18	0.07	0.02
Data collection range	$(r/a)_{\min}$	0.07	$(r/a)_{\max}$	0.70	

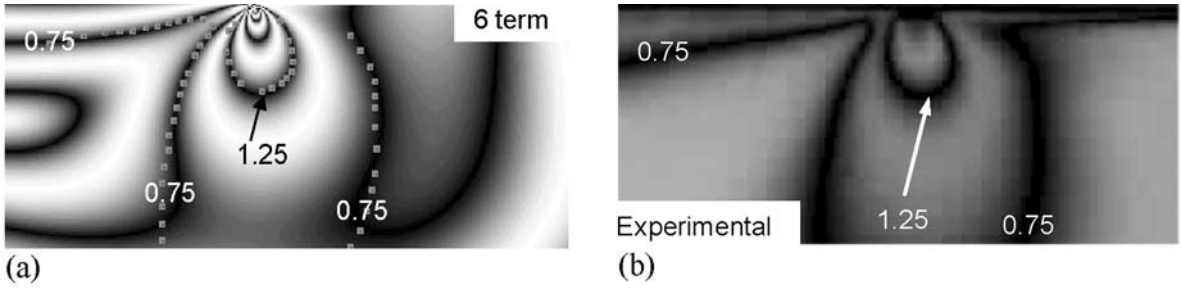

Fig. 6 Comparison between (b) the experimental image and (a) the reconstructed image obtained using the experimentally obtained parameters (six-term solution) with data points echoed for the epoxy material side problem given in Fig. 3(d)

appropriately changed (Table 4) so as to obtain for any crack orientation sufficient fringes without contradicting the model. By changing θ', the loading is changed from predominantly mode I to predominantly mode II. Figure 7 shows the comparison of the experimental image with the reconstructed fringe patterns for various crack orientations of the PSM1–epoxy bimaterial pair. Figures 7(a) and (b) are for $\theta' = 75^\circ$ (74.9°), Figs 7(c) and (d) are for $\theta' = 45^\circ$ (44.4°), and Figs 7(e) and (f) are for $\theta' = 30^\circ$ (29.5°). For the first two cases, a seven-term solution is found to be necessary and for the last case a five-term solution is found to be sufficient. Figure 8 shows the results for the epoxy–mild steel bimaterial pair. Figures 8(a) and (b) are for $\theta' = 90^\circ$ (89.8°), Figs 8(c) and (d) are for $\theta' = 75^\circ$ (74.9°), Figs 8(e) and (f) are for $\theta' = 45^\circ$ (44.4°), and

Table 4 Salient results obtained by the new methodology for different crack orientations and for two values of ε

	θ'	Load (N)	$(r/a)_{\min}$	$(r/a)_{\max}$	$\lvert K\rvert$ (MPa m$^{1/2}$)	Phase angle (deg)	$\lvert K\rvert^* \times 10^{-7}$ (m$^{1/2}$)
PSM1–epoxy,	90 (89.9)	205	0.11	0.65	0.191	−10.54	3.13
$\varepsilon = 0.01$	75 (74.9)	205	0.08	0.85	0.174	−21.98	2.85
	45 (44.4)	123	0.07	0.57	0.045	−69.15	1.37
	30 (29.5)	123	0.11	0.94	0.065	−89.16	1.23
Epoxy–mild steel,	90 (89.9)	328	0.07	1.05	0.212	9.77	2.33
$\varepsilon = 0.1$	75 (75.8)	328	0.07	0.87	0.214	15.47	2.35
	45 (45.8)	205	0.05	0.87	0.087	−68.65	1.53
	30 (30.2)	246	0.05	0.86	0.124	−62.2	1.82

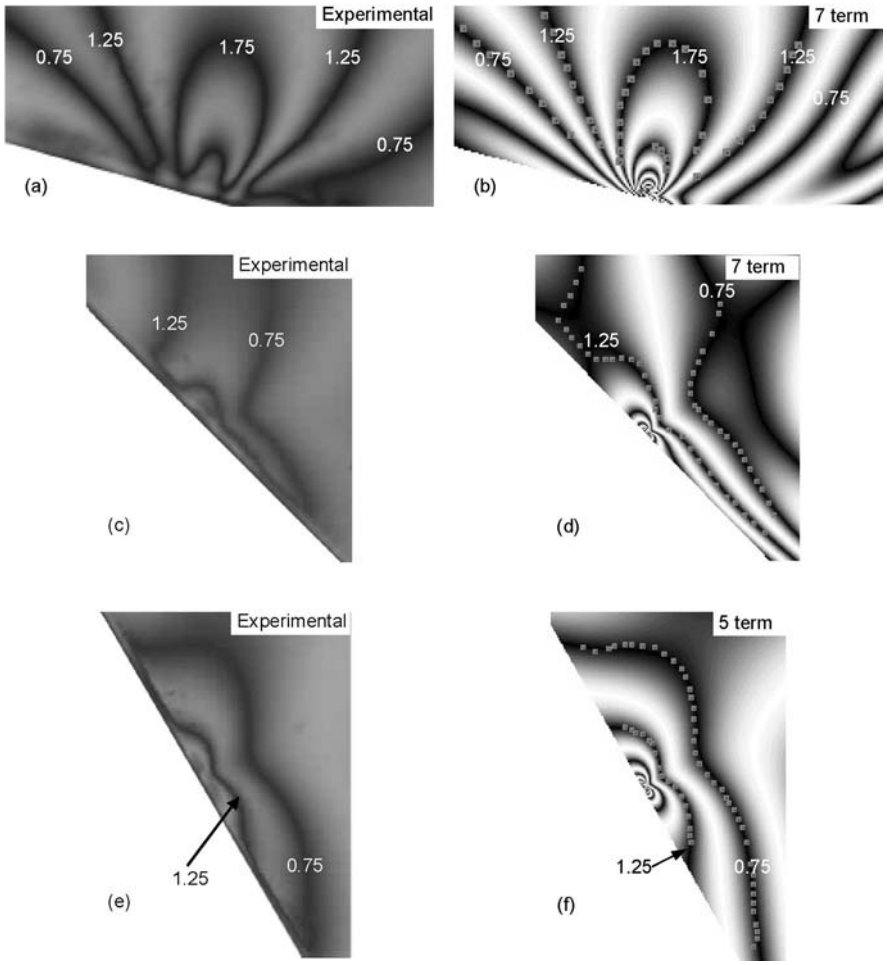

Fig. 7 Comparison between (a), (c), (e) the experimental images and (b), (d), (f) the theoretically reconstructed images obtained using the experimentally obtained parameters with data points echoed for $\varepsilon = 0.01$: (a) experimental image for $\theta' = 75^\circ$ (74.9°); (b) reconstructed for the seven-term solution; (c) experimental image for $\theta' = 45^\circ$ (44.4°); (d) reconstructed for the seven-term solution; (e) experimental image for $\theta' = 30^\circ$ (29.5°); (f) reconstructed for the five-term solution

Figs 8(g) and (h) are for $\theta' = 30^\circ$ (30.24°). The number of terms required differs here for each case. It can be seen that the use of six to eight terms is required in the series to obtain a satisfactory solution. In all the crack orientations considered and for both the bimaterial pairs, the theoretically simulated fringe pattern has captured the various geometric features of the fringe field. This result indirectly validates the applicability of the multi-parameter stress field developed in section 2.3 for various mode mixities and for different bimaterial constants.

The modulus of the complex SIF and its phase angle $\tan^{-1}(K_{\mathrm{II}}/K_{\mathrm{I}})$ evaluated for different crack orientations and for two values of ε are given in Table 4. The table also shows the normalized $|K|$ defined by

$$|K|^* = \frac{|K|}{P/dh} \tag{15}$$

where P is the applied load, d is the diameter of the bimaterial disc, and h is the thickness of the model. The variations in normalized $|K|$ ($|K|^*$) and phase angle with respect to various loading angles are presented for two bimaterial constants ε and are shown in Figs 9 and 10 respectively.

5 CONCLUSION

The stress field parameters in the neighbourhood of an interface crack tangential to the interface in a bimaterial are evaluated by a multi-parameter stress field equation in a least-squares sense for the first time. For the problems discussed, in the multi-parameter stress field equation, five (total ten) to eight (total 16) terms in the series are required to model the stress field. The number of terms required is problem dependent and it has to be obtained by

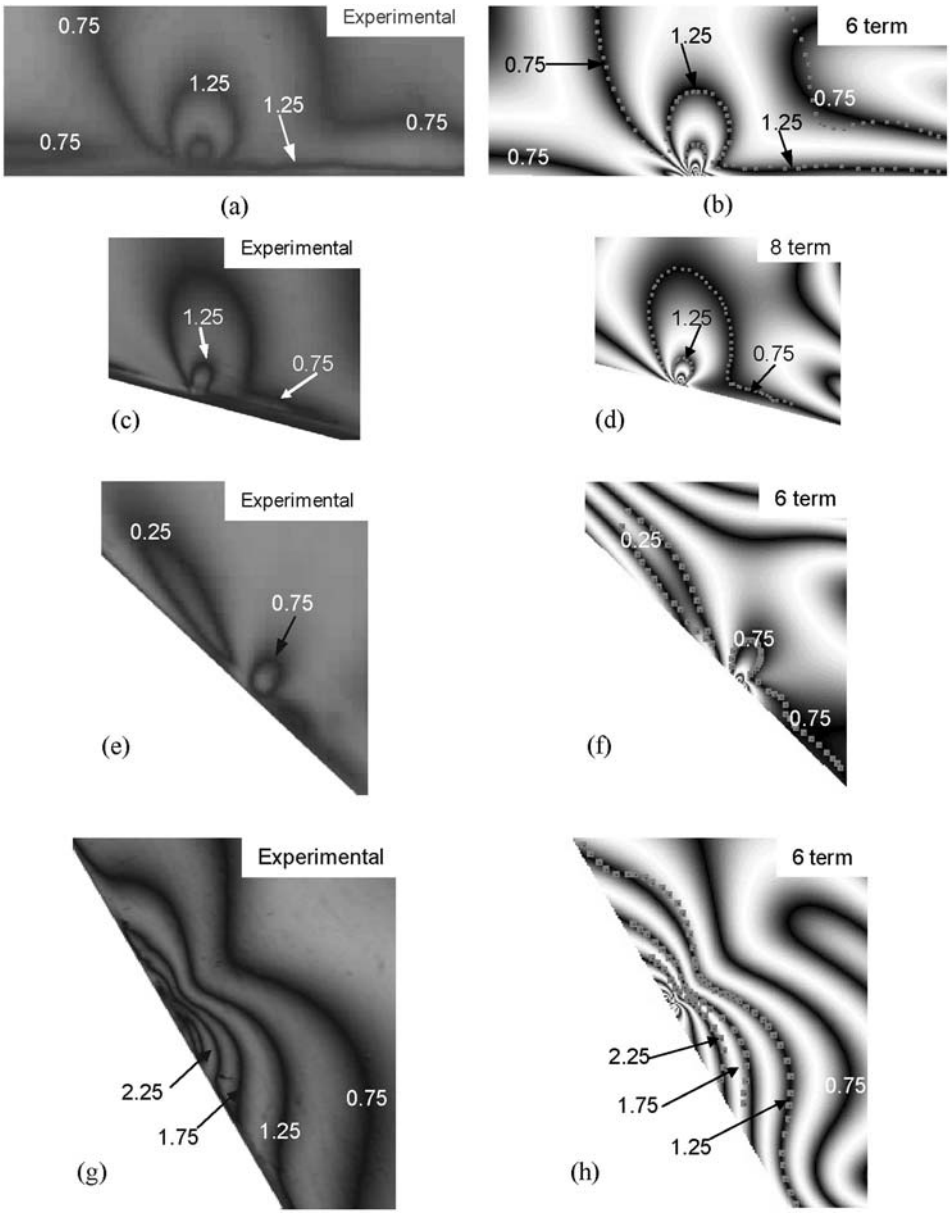

Fig. 8 Comparison between (a), (c), (e), (g) the experimental images and (b), (d), (f), (h) the theoretically reconstructed images obtained using the experimentally obtained parameters with data points echoed for $\varepsilon = 0.1$: (a) experimental image for $\theta' = 90^\circ$ (89.8°); (b) reconstructed for the six-term solution; (c) experimental image for $\theta' = 75^\circ$ (74.9°); (d) reconstructed for the eight-term solution; (e) experimental image for $\theta' = 45^\circ$ (44.4°); (f) reconstructed for the six-term solution; (g) experimental image for $\theta' = 30^\circ$ (30.24°); (h) reconstructed for the six-term solution

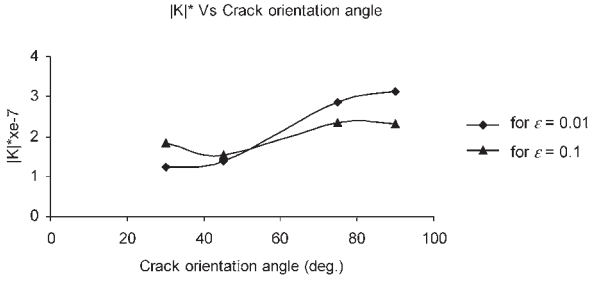

Fig. 9 Graph showing the normalized $|K|$ as a function of the crack orientation angle for two ε

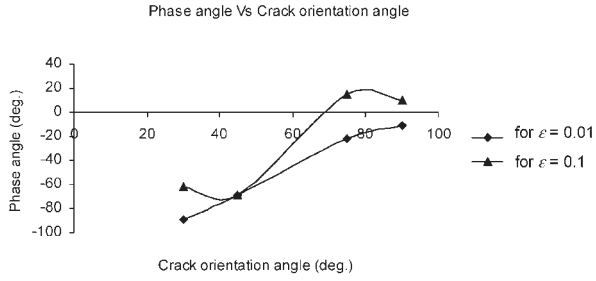

Fig. 10 Graph showing the phase angle as a function of crack orientation angle for two ε

employing the least-squares procedure. A convergence error (fringe order error minimization) value of less than 0.05 is found to be sufficient for most of the problems considered. The zone of data collection is problem dependent and does not have an angular dependence like the singular term solution (the constant-radius method [**4**]). The range from $(r/a)_{\min}$ to $(r/a)_{\max}$ for the problems considered is from 0.05 to 1.05, which indicates that the zone of data collection is reasonable for experimental evaluation. The sample bimaterial pairs selected in this work covers a wide range of ε (from 0.01 to 0.1). It may be worthwhile to note that, for bimaterial ceramic pairs, the range of ε is only from 0.01 to 0.03 [**8**]. The multi-parameter stress field solution has faithfully captured the experimental features of the fringes for different mode mixities and for two values of ε. This indirectly validates the correctness of the multi-parameter stress field equation developed.

REFERENCES

1 **Williams, M. L.** The stresses around a fault or crack in dissimilar media. *Bull. Seismol. Soc. America*, 1959, **49**(2), 199–204.
2 **Erdogan, E.** Stress distribution in a non-homogeneous elastic plane with cracks. *Tran. ASME, J. Appl. Mechanics*, 1963, **85**, 232–236.
3 **Comninou, M.** An overview of interface cracks. *Engng Fracture Mechanics*, 1990, **37**(1), 197–208.
4 **Lu, H.** and **Chiang, F. P.** Photoelastic determination of stress intensity factor of an interfacial crack in a bi-material. *Tran. ASME, J. Appl. Mechanics*, 1993, **60**, 93–100.
5 **Soh, A.-K.** An improved photo-elastic technique for determining the mixed mode stress intensity factors for interfacial cracks in a bi-material. *Composites Sci. Technol.*, 1999, **59**, 1033–1039.
6 **Ramesh, K., Gupta, S.,** and **Kelkar, A. A.** Evaluation of stress field parameters in fracture mechanics by photoelasticity-revisited. *Engng Fracture Mechanics*, 1997, **56**(1), 25–45.
7 **Symington, M. F.** Eigenvalues for interface cracks in linear elasticity. *Trans. ASME, J. Appl. Mechanics*, 1987, **54**, 973–974.
8 **Rice, J. R.** Elastic fracture mechanics concepts for interfacial cracks. *Tran. ASME, J. Appl. Mechanics*, 1988, **55**, 98–103.
9 **Deng, X.** General crack-tip fields for stationary and steadily growing interface cracks in anisotropic bimaterials. *Trans. ASME, J. Appl. Mechanics*, 1993, **60**, 183–189.
10 **Rice, J. R.** and **Sih, G. C.** Plane problems of cracks in dissimilar media. *Trans. ASME, J. Appl. Mechanics*, 1965, **32**, 418–423.
11 **Hutchinson, J. W., Mear, M. E.,** and **Rice, J. R.** Crack paralleling an interface between dissimilar materials. *Trans. ASME, J. Appl. Mechanics*, 1987, **54**, 828–832.
12 **Shih, C. F.** and **Asaro, R. J.** Elastic–plastic analysis of cracks on bi-material interfaces. Part I: small scale yielding. *Trans. ASME, J. Appl. Mechanics*, 1988, **55**, 299–316.
13 **Wang, J. S.** and **Suo, Z.** Experimental determination of interfacial toughness curves using brazil-nut-sandwiches. *Acta Metallurgica Materia*, 1990, **38**, 1279–1290.
14 **Ravichandran, M.** Evaluation of stress intensity factors for an interface crack in a bi-material using digital photoelasticity. MS thesis, Department of Applied Mechanics, Indian Institute of Technology, Madras, India, December 2003.
15 **Atluri, S. N.** and **Kobayashi, A. S.** Mechanical response of materials. In *Handbook on Experimental Mechanics*, 1987, pp. 1–37 (Prentice-Hall, Englewood Cliffs, New Jersey); 1993 (SEM, Bethel, Connecticut).
16 **Chona, R., Irwin, G. R.,** and **Sanford, R. J.** Influence of specimen size and shape on the singularity dominated zone. In Proceedings of the 14th National Symposium on *Fracture Mechanics*, ASTM Special Technical Publication 791, 1983, pp. 13–123 (American Society for Testing and Materials, Philadelphia, Pennsylvania).
17 **Ramesh, K.** *Digital Photoelasticity: Advanced Techniques and Applications*, 2000 (Springer-Verlag, Berlin).
18 **Ramesh, K.** and **Pramod, B. R.** Digital image processing of fringe patterns in photomechanics. *Opt. Engng*, 1992, **31**(7), 1487–1498.
19 **Ramesh, K.** and **Singh, R. K.** Comparative performance evaluation of various fringe-thinning algorithms in photomechanics. *J. Elect. Imaging*, 1995, **4**(1), 71–83.
20 **Ravichandran, M.** and **Ramesh, K.** Determination of stress intensity factors for an interface crack in a bi-material by digital photoelasticity. *Advances in Experimental Mechanics, Applied Mechanics and Materials*, Vols 1, 2, 2004, pp. 139–146 (Trans. Tech, Aedermannsdorf).

APPENDIX 1

Notation

$2a$	crack length
a_n	complex constant used in the power series $f(z)$
b_n	complex constant used in the power series $g(z)$
c_i	$= (1 + \kappa_i)/G_i$
d	diameter of the Brazilian disc
D_i	material constant for region i
E_i	Young's modulus of material i
$f(z)$	power series used in Rice's analytic function $\psi_j(z)$ and $\chi_j(z)$
F_σ	material stress fringe value
g_m	least-squares function defined for the mth data point
$g(z)$	power series used in Rice's analytic function $\psi_j(z)$ and $\chi_j(z)$

G_j	shear modulus of material j
h	thickness of model
k_n	complex coefficients in Deng's equation
$k_1 + \mathrm{i}k_2$	complex stress intensity factor used by Sih and Rice having units of MPa $\mathrm{m}^{1/2}\,\mathrm{m}^{-\mathrm{i}\varepsilon}$
$K_1 + \mathrm{i}K_2$	complex stress intensity factor having units of MPa $\mathrm{m}^{1/2}\,\mathrm{m}^{-\mathrm{i}\varepsilon}$
$K_\mathrm{I} + \mathrm{i}K_\mathrm{II}$	complex stress intensity factor having units of MPa $\mathrm{m}^{1/2}$
L	characteristic length
N	fringe order
N_exp	experimental fringe order
N_theory	theoretical value of the fringe order
P	load applied
Q	$= 2\sqrt{2\pi}\cosh(\pi\varepsilon)$
r	radial distance measured from the crack tip
R	$= \sqrt{2\pi}(1+w)$
S	$= \mathrm{e}^{-\varepsilon(\pi-\theta)}$
T	magnitude of the traction vector
w	$= (1+\kappa_1)G_2/(1+\kappa_2)G_1$
z	complex number representation $= x + \mathrm{i}y$
ε	bimaterial constant
θ	angular orientation of the point of interest measured from the crack tip
θ'	orientation of the crack with respect to the point of load application
κ_j	$= (3-\nu_j)/(1+\nu_j)$ for plane stress and $3-4\nu_j$ for plane strain $(j = 1, 2)$
ν_j	Poisson's ratio of material j
$\hat{\sigma}_n^\mathrm{I}(\theta), \hat{\sigma}_n^\mathrm{II}(\theta)$	angular functions of the stress field used in Deng's equation
$\sigma_{rr}, \sigma_{\theta\theta}, \tau_{r\theta}$	stress components in polar coordinates
$\sigma_{xx}, \sigma_{yy}, \tau_{xy}$	stress components in Cartesian coordinates
σ_{xy}^∞	remote uniform shear stress
σ_{yy}^∞	remote uniform tensile stress
σ_{0x}	constant stress term in the σ_x stress component
$\sigma_1 - \sigma_2$	principal stress difference
χ	Muskhelishvili analytic function
ψ	Muskhelishvili analytic function
ω	direction of traction T

APPENDIX 2

The Muskhelishvili representation of stresses in two-dimensional elasticity is given by

$$\sigma_{rr} + \sigma_{\theta\theta} = 4\mathrm{Re}[\psi'(z)]$$
$$\sigma_{\theta\theta} - \sigma_{rr} + 2\mathrm{i}\tau_{r\theta} = 2\,\mathrm{e}^{\mathrm{i}2\theta}[(\bar{z}-z)\psi''(z) - \psi'(z) + \chi'(z)] \tag{16}$$

where $\psi(z)$ and $\chi(z)$ are analytic functions. The function $\psi'(z)$ and $\chi'(z)$ have been given by Rice [**8**] as

$$\psi_1'(z) = \mathrm{e}^{-\varepsilon\pi}\, z^{-1/2-\mathrm{i}\varepsilon} f(z) + 2D_1 g(z)$$
$$\chi_1'(z) = \mathrm{e}^{\varepsilon\pi}\, z^{-1/2+\mathrm{i}\varepsilon} \bar{f}(z) - 2D_1 \bar{g}(z) \tag{17}$$

for material 1 (Fig. 1), and

$$\psi_2'(z) = \mathrm{e}^{\varepsilon\pi}\, z^{-1/2-\mathrm{i}\varepsilon} f(z) + 2D_2 g(z)$$
$$\chi_2'(z) = \mathrm{e}^{-\varepsilon\pi}\, z^{-1/2+\mathrm{i}\varepsilon} \bar{f}(z) - 2D_2 \bar{g}(z) \tag{18}$$

for material 2 (Fig. 1), where

$$c_i = \frac{1+\kappa_i}{G_i}, \qquad D_1 = \frac{c_2}{c_1+c_2}, \qquad D_2 = \frac{c_1}{c_1+c_2}$$

The functions $f(z)$ and $g(z)$ are taken as the power series

$$f(z) = \sum_{n=0}^{\infty} a_n z^n \tag{19a}$$

$$g(z) = \sum_{n=0}^{\infty} b_n z^n \tag{19b}$$

where a_n and b_n are complex constants. The first term a_0 in the series in equation (19a) represents the strength of the crack-tip singularity and is related to complex stress intensity factor K by

$$a_0 = \frac{\bar{K}}{2\sqrt{2\pi}\cosh(\pi\varepsilon)} \tag{20}$$

The real and imaginary parts of the complex constant a_0 are represented by the superscripts R and I and the overbar denotes the complex conjugate according to

$$a_0 = a_0^\mathrm{R} + \mathrm{i}a_0^\mathrm{I} = \frac{K_1 - \mathrm{i}K_2}{2\sqrt{2\pi}\cosh(\pi\varepsilon)} \tag{21}$$

The complex coefficient b_0 in equation (19b) represents a stress field of type σ_{0x} which is uniform but different in each of the two materials. Reference [**14**] gave the details for expressing the stress field in a compact form. The multi-parameter stress field equations in polar coordinates corresponding to

material 1 are

$$
\begin{aligned}
(\sigma_{rr})_1 = & \sum_{n=0}^{\infty} a_n^{\mathrm{I}} r^{n-1/2} (\mathrm{e}^{-\varepsilon(\pi-\theta)} \{2\cos[(n-\tfrac{1}{2})\theta - \varepsilon \ln r] + \cos[(n+\tfrac{3}{2})\theta - \varepsilon \ln r] \\
& \qquad + (1-2n)\sin\theta \sin[(n+\tfrac{1}{2})\theta - \varepsilon \ln r] + 2\varepsilon \sin\theta \cos[(n+\tfrac{1}{2})\theta - \varepsilon \ln r]\} \\
& \qquad - \mathrm{e}^{\varepsilon(\pi-\theta)} \cos[(n+\tfrac{3}{2})\theta + \varepsilon \ln r]) \\
& + \sum_{n=0}^{\infty} a_n^{\mathrm{II}} r^{n-1/2} (\mathrm{e}^{-\varepsilon(\pi-\theta)} \{-2\sin[(n-\tfrac{1}{2})\theta - \varepsilon \ln r] - \sin[(n+\tfrac{3}{2})\theta - \varepsilon \ln r] \\
& \qquad + (1-2n)\sin\theta \cos[(n+\tfrac{1}{2})\theta - \varepsilon \ln r] - 2\varepsilon \sin\theta \sin[(n+\tfrac{1}{2})\theta - \varepsilon \ln r]\} \\
& \qquad - \mathrm{e}^{\varepsilon(\pi-\theta)} \sin[(n+\tfrac{3}{2})\theta + \varepsilon \ln r]) \\
& + \sum_{n=0}^{\infty} 4D_1 b_n^{\mathrm{I}} r^n \{\cos(n\theta) + \cos[(n+2)\theta] - n\sin\theta \sin[(n+1)\theta]\} \\
& + \sum_{n=0}^{\infty} 4D_1 b_n^{\mathrm{II}} r^n \{-\sin(n\theta) - n\sin\theta \cos[(n+1)\theta]\}
\end{aligned} \tag{22a}
$$

$$
\begin{aligned}
(\sigma_{\theta\theta})_1 = & \sum_{n=0}^{\infty} a_n^{\mathrm{I}} r^{n-1/2} (\mathrm{e}^{-\varepsilon(\pi-\theta)} \{2\cos[(n-\tfrac{1}{2})\theta - \varepsilon \ln r] + \cos[(n+\tfrac{3}{2})\theta - \varepsilon \ln r] \\
& \qquad - (1-2n)\sin\theta \sin[(n+\tfrac{1}{2})\theta - \varepsilon \ln r] - 2\varepsilon \sin\theta \cos[(n+\tfrac{1}{2})\theta - \varepsilon \ln r]\} \\
& \qquad - \mathrm{e}^{\varepsilon(\pi-\theta)} \cos[(n+\tfrac{3}{2})\theta + \varepsilon \ln r]) \\
& + \sum_{n=0}^{\infty} a_n^{\mathrm{II}} r^{n-1/2} (\mathrm{e}^{-\varepsilon(\pi-\theta)} \{-2\sin[(n-\tfrac{1}{2})\theta - \varepsilon \ln r] - \sin[(n+\tfrac{3}{2})\theta - \varepsilon \ln r] \\
& \qquad - (1-2n)\sin\theta \cos[(n+\tfrac{1}{2})\theta - \varepsilon \ln r] + 2\varepsilon \sin\theta \sin[(n+\tfrac{1}{2})\theta - \varepsilon \ln r]\} \\
& \qquad - \mathrm{e}^{\varepsilon(\pi-\theta)} \sin[(n+\tfrac{3}{2})\theta + \varepsilon \ln r]) \\
& + \sum_{n=0}^{\infty} 4D_1 b_n^{\mathrm{I}} r^n \{\cos(n\theta) - \cos[(n+2)\theta] + n\sin\theta \sin[(n+1)\theta]\} \\
& + \sum_{n=0}^{\infty} 4D_1 b_n^{\mathrm{II}} r^n \{-\sin(n\theta) + n\sin\theta \cos[(n+1)\theta]\}
\end{aligned} \tag{22b}
$$

$$
\begin{aligned}
(\tau_{r\theta})_1 = & \sum_{n=0}^{\infty} a_n^{\mathrm{I}} r^{n-1/2} (\mathrm{e}^{-\varepsilon(\pi-\theta)} \{-\sin[(n+\tfrac{3}{2})\theta - \varepsilon \ln r] + (1-2n)\sin\theta \cos[(n+\tfrac{1}{2})\theta - \varepsilon \ln r] \\
& \qquad - 2\varepsilon \sin\theta \sin[(n+\tfrac{1}{2})\theta - \varepsilon \ln r]\} + \mathrm{e}^{\varepsilon(\pi-\theta)} \sin[(n+\tfrac{3}{2})\theta + \varepsilon \ln r]) \\
& + \sum_{n=0}^{\infty} a_n^{\mathrm{II}} r^{n-1/2} (\mathrm{e}^{-\varepsilon(\pi-\theta)} \{-\cos[(n+\tfrac{3}{2})\theta - \varepsilon \ln r] - (1-2n)\sin\theta \sin[(n+\tfrac{1}{2})\theta - \varepsilon \ln r] \\
& \qquad - 2\varepsilon \sin\theta \cos[(n+\tfrac{1}{2})\theta - \varepsilon \ln r]\} - \mathrm{e}^{\varepsilon(\pi-\theta)} \cos[(n+\tfrac{3}{2})\theta - \varepsilon \ln r]) \\
& + \sum_{n=0}^{\infty} 4D_1 b_n^{\mathrm{I}} r^n \{-n\sin\theta \cos[(n+1)\theta] - \sin[(n+2)\theta]\} + \sum_{n=0}^{\infty} 4D_1 a_n^{\mathrm{II}} r^n \{n\sin\theta \sin[(n+1)\theta]\}
\end{aligned} \tag{22c}
$$

The stress field expressions for material 2 can be obtained by replacing $e^{-\varepsilon\pi}$ by $\mathrm{e}^{\varepsilon\pi}$, $\mathrm{e}^{\varepsilon\pi}$ by $\mathrm{e}^{-\varepsilon\pi}$, and D_1 by D_2 in equations (22) [see equations (17) and (18)].